

Cumulant expansion for the treatment of light–matter interactions in arbitrary material structures

Cite as: *J. Chem. Phys.* **152**, 034108 (2020); doi: [10.1063/1.5138937](https://doi.org/10.1063/1.5138937)

Submitted: 15 November 2019 • Accepted: 7 January 2020 •

Published Online: 17 January 2020



View Online



Export Citation



CrossMark

M. Sánchez-Barquilla,  R. E. F. Silva,  and J. Feist^{a)} 

AFFILIATIONS

Departamento de Física Teórica de la Materia Condensada and Condensed Matter Physics Center (IFIMAC), Universidad Autónoma de Madrid, E-28049 Madrid, Spain

Note: This paper is part of the JCP Special Topic on Emerging Directions in Plasmonics.

^{a)} Author to whom correspondence should be addressed: johannes.feist@uam.es

ABSTRACT

Strong coupling of quantum emitters with confined electromagnetic modes of nanophotonic structures may be used to change optical, chemical, and transport properties of materials, with significant theoretical effort invested toward a better understanding of this phenomenon. However, a full theoretical description of both matter and light is an extremely challenging task. Typical theoretical approaches simplify the description of the photonic environment by describing it as a single mode or few modes. While this approximation is accurate in some cases, it breaks down strongly in complex environments, such as within plasmonic nanocavities, and the electromagnetic environment must be fully taken into account. This requires the quantum description of a continuum of bosonic modes, a problem that is computationally hard. We here investigate a compromise where the quantum character of light is taken into account at modest computational cost. To do so, we focus on a quantum emitter that interacts with an arbitrary photonic spectral density and employ the cumulant, or cluster, expansion method to the Heisenberg equations of motion up to first, second, and third order. We benchmark the method by comparing it with exact solutions for specific situations and show that it can accurately represent dynamics for many parameter ranges.

Published under license by AIP Publishing. <https://doi.org/10.1063/1.5138937>

I. INTRODUCTION

Light–matter interaction is of paramount importance for unraveling the laws of nature, and its deep understanding allows us to control and manipulate physical and chemical systems. In particular, one can modify the properties of a quantum emitter simply by changing its electromagnetic environment, for example, by enclosing it within an optical cavity. This may give rise to a change in the decay rate for spontaneous emission in the weak coupling regime, the so-called Purcell effect,¹ or to the appearance of hybrid light–matter states, the so-called polaritons, in the strong-coupling regime.^{2–5} Over the last few decades, it has been shown that strong light–matter coupling can be achieved using a large variety of physical implementations as the “cavity” that provides the electromagnetic field confinement. These include Fabry–Perot

cavities consisting of two mirrors,⁵ propagating surface plasmon polaritons,⁶ plasmonic hole,⁷ and nanoparticle arrays,⁸ isolated plasmonic nanoparticles,⁹ and nanoparticle-on-mirror geometries,^{10,11} as well as hybrid cavities combining plasmonic and dielectric materials.^{12–14} In many of these systems, the electromagnetic field modes are not well-described by isolated lossy cavity modes, and a correct treatment demands theoretical approaches that are able to deal with the complexity of the electromagnetic field modes and their spectrum.

In principle, to treat the problem of light–matter interaction, one can rely on the most general theory that describes light and matter on equal footing, i.e., quantum electrodynamics (QED).¹⁵ However, treating all light and matter degrees of freedom in the systems described above in a quantum mechanical way is an intractable problem and approximations must be performed. One of the most

common assumptions in quantum optics is to consider that the material system of interest only interacts with a single mode of the electromagnetic (EM) field, with the interaction typically treated within the dipole approximation. This leads to the Rabi,¹⁶ Dicke,¹⁷ Jaynes–Cummings,¹⁸ and Tavis–Cummings¹⁹ models depending on the number of treated emitters and the approximations performed,^{20–24} all of which have been successfully used and extended to describe a wide variety of experimental implementations. Nevertheless, as discussed above, the simplification to a single (or few) quantized light modes in the treatment of the electromagnetic field is not always a good approximation.

In some cases, the quantum character of the electromagnetic field may be neglected and it is possible to rely on Maxwell’s equations. In such mean-field approaches, the classical EM field is then coupled to the dipole of the quantum emitters and the coupled Maxwell–Schrödinger or Maxwell–Bloch equations are solved.^{25,26} This approach, in principle, allows for the description of arbitrary photonic structures but misses all effects due to the quantization of the EM field, such as spontaneous emission. Recently, several groups have extended these approaches to allow for a more complete description, based on, e.g., an Ehrenfest+Relaxation approach^{27,28} or cavity quantum electrodynamics with multi-trajectory Ehrenfest dynamics.²⁹

In cases that a full quantum description is desired, a strategy has to be used to quantize the EM field modes in the presence of material bodies. This is possible for simple geometries using a variety of strategies.^{11,30,31} For systems with a few, but possibly interfering, resonances, it was recently shown how to quantize the corresponding quasi-normal modes as lossy cavity modes.¹³ For arbitrary material structures, the most general solution is given by the framework of macroscopic QED,^{32–35} which was developed in the last few decades to circumvent the problems that arise when applying the rules of canonical quantization in the presence of linear, dispersive, and absorbing materials. Within this framework, which we use as the basis for our numerical approach below, the medium-supported electromagnetic field is formally generated by local bosonic dynamical operators $\hat{\mathbf{f}}(\mathbf{r}, \omega)$ at every point in space and frequency, with the EM field obtained through a convolution of the EM Green’s function. While the sheer number of formal modes prevents their direct use in a “standard” description, a large number of relevant observables and effects can be obtained in approaches where these degrees of freedom are integrated out in some sense, with final expressions only depending on the EM Green’s function after performing a perturbation expansion or treating few-level emitters approximately as bosonic degrees of freedom.^{35–39}

Even for the case of nonperturbative interactions between several emitters and arbitrary photonic structures, it was realized by Buhmann and Welsch,⁴⁰ and later independently by several other groups,^{41,42} that a unitary frequency-dependent basis transformation can be used to transform the local operators $\hat{\mathbf{f}}(\mathbf{r}, \omega)$ to a set of new modes in such a way that only a *single* photonic mode interacts with each emitter at each frequency, with the strength of the interaction encoded in the spectral density, $J(\mathbf{r}, \omega)$ at the position \mathbf{r} of the emitter. We note that one naturally arrives at the same picture by calculating the local density of EM states and using its relation with the decay rate and the dyadic Green’s function.⁴³

When the spectral density has a Lorentzian profile, the dynamics can be mapped to the dissipative Rabi model.^{22,44} Generalizing this idea, if the spectral density is well approximated as a sum of N Lorentzians, the dynamics can be fully solved by including N dissipative bosonic modes.^{11,39,45} However, for arbitrary complex spectral densities, this approximation is not useful. In that case, one approach is to exploit the tools developed for open quantum systems,^{20,21,46} which exactly describe a quantum system coupled to a continuous “bath” described by a given spectral density. In particular, if the coupling between the system and the bath is weak, one can apply the Markov approximation (which assumes that the bath has “no memory”), such that the EM environment simply introduces a frequency-dependent decay rate (corresponding exactly to the Purcell effect). When this approximation is not applicable, more advanced numerical approaches such as tensor network calculations^{47,48} or hierarchical equations of motion⁴⁹ can be employed, possibly after a chain transformation of the associated Hamiltonian.⁵⁰ Such approaches have been used to study static properties and dynamics in organic polaritons.^{51,52} However, these are numerically demanding approaches that require significant computational resources.

In this work, we explore an intermediate approach that goes beyond a mean-field description, without trying to obtain a full quantum description of the coupled emitter–photon system. We do so by employing the cumulant or cluster expansion method^{53–55} to treat the interaction of a single quantum emitter with an arbitrary photonic spectral density. This method has its roots in the Bogoliubov–Born–Green–Kirkwood–Yvon (BBGKY) hierarchy.⁵⁵ It relies on the fact that for a system of interacting particles, the dynamics of the mean value of an N -particle operator depend on the mean values of $N + 1$ -particle operators. Truncating this description by neglecting operator correlations above some order leads to a closed set of equations. This method was already applied in the context of cavity QED,^{56–59} but a systematic study of the importance of the different terms appearing in the expansion has not been provided yet. We here present an extensive study of how different truncations of the cumulant expansion perform in the computation of the dynamics of the quantum emitter and EM modes. In particular, we investigate the effect of truncating the cumulant expansion at different orders and compare different strategies for performing these truncations. To benchmark our method, we choose spectral densities for which (almost) exact solutions can be obtained through the Wigner–Weisskopf (WW) and dissipative Rabi model, respectively.

II. METHOD

Within the framework of macroscopic QED, the Hamiltonian that describes the interaction between one emitter and a medium-assisted electromagnetic field is, within the dipole approximation⁴⁰ (here and in the following, we use units where $\hbar = 1$),

$$H = \sum_{\lambda=e,m} \int d\mathbf{r}^3 \int_0^\infty d\omega \omega \mathbf{f}_\lambda^\dagger(\mathbf{r}, \omega) \mathbf{f}_\lambda(\mathbf{r}, \omega) + H_{\text{em}} - \hat{\boldsymbol{\mu}} \cdot \mathbf{E}(\mathbf{r}_A), \quad (1)$$

where $f_\lambda(\mathbf{r}, \omega)$ and $f_\lambda^\dagger(\mathbf{r}, \omega)$ are the bosonic annihilation and creation operators, H_{em} is the bare-emitter Hamiltonian, $\hat{\boldsymbol{\mu}}$ is the dipole operator of the two-level system, and $\mathbf{E}(\mathbf{r}_A)$ is the electric field operator,

which is given by a superposition of the bosonic operators $\hat{f}_\lambda(\mathbf{r}, \omega)$ with weights determined by the classical Green's tensor $\mathbf{G}(\mathbf{r}_A, \mathbf{r}, \omega)$. As mentioned above, a frequency-dependent unitary transformation of $f_\lambda(\mathbf{r}, \omega)$ can be performed such that for each frequency, only a *single* photonic mode $a(\omega)$ interacts with the emitter⁴⁰ (under the assumption that only a single polarization direction interacts with the emitter dipole operator). Furthermore, we here approximate the quantum emitter as a two-level system described by the Pauli matrices σ^i ($i \in \{x, y, z\}$), with transition frequency Ω_0 and transition dipole moment $\boldsymbol{\mu}$. The Hamiltonian then becomes

$$H = \int_0^\infty d\omega \omega a^\dagger(\omega) a(\omega) + \frac{\Omega_0}{2} \sigma^z + \int_0^\infty d\omega g(\omega) (a^\dagger(\omega) + a(\omega)) \sigma^x, \quad (2)$$

where $g(\omega)$ is the coupling between the emitter and the electromagnetic modes,

$$g(\omega) = \sqrt{\frac{\mu_0}{\pi} \omega^2 \boldsymbol{\mu} \cdot \text{Im} \mathbf{G}(\mathbf{r}_A, \mathbf{r}_A, \omega) \cdot \boldsymbol{\mu}}, \quad (3)$$

where \mathbf{r}_A is the position of the emitter. The expression inside the square root in Eq. (3) is the spectral density $J(\mathbf{r}, \omega)$. For the numerical implementation, we discretize the frequency integrals on a grid with regular spacing $\Delta\omega$. Formally, we define the discrete orthonormal modes,

$$a_n = \frac{1}{\sqrt{\Delta\omega}} \int_{n\Delta\omega}^{(n+1)\Delta\omega} a(\omega) d\omega, \quad (4)$$

which obey $[a_n, a_m^\dagger] = \delta_{nm}$ since the original continuum modes obey $[a(\omega), a^\dagger(\omega')] = \delta(\omega - \omega')$. This leads to the discrete Hamiltonian,

$$H_d = \sum_n \omega_n a_n^\dagger a_n + \frac{\Omega_0}{2} \sigma^z + \sum_n g_n (a_n^\dagger + a_n) \sigma^x, \quad (5)$$

where $\omega_n = (n + \frac{1}{2})\Delta\omega$ and $g_n = \sqrt{J(\mathbf{r}_A, \omega_n)\Delta\omega}$. Here, we have discarded the (infinite number of) superpositions of $a(\omega)$ orthogonal to a_n in each interval that would make the transformation unitary. Formally, this discretization can be understood as a chain transformation^{50,60} of the continuum modes within each interval $[n\Delta\omega, (n+1)\Delta\omega]$ under the approximation that $g(\omega)$ is constant within it, discarding all but the first chain site.

In order to describe the action of an incoming classical electromagnetic field (e.g., a laser pulse), it would be possible to simply use a product of coherent states as the initial wave function, $|\psi(0)\rangle = \prod_n |\alpha_n(0)\rangle = \prod_n e^{\alpha_n(0)a_n^\dagger - \alpha_n(0)^* a_n} |0\rangle$, where $\alpha_n(0)$ correspond to the classical amplitudes of the modes when expressing the laser pulse in the basis defined by these modes. In order to avoid the necessity for explicitly propagating this classical field within the quantum calculation, the classical and the quantum field can be split in the Hamiltonian using a time-dependent displacement operator¹⁵ $T(t) = e^{\sum_n \alpha_n^*(t) a_n - \alpha_n(t) a_n^\dagger}$, where $\alpha_n(t) = \alpha_n(0) e^{-i\omega_n t}$. Applying this transformation to the wavefunction, $|\psi'\rangle = T(t)|\psi\rangle$, corresponds to transforming the Hamiltonian as

$$\begin{aligned} H'_d &= T(t) H_d T^\dagger(t) - iT(t) \partial_t T^\dagger(t) \\ &= \sum_n \omega_n a_n^\dagger a_n + \frac{\Omega_0}{2} \sigma^z + \sum_n g_n (a_n^\dagger + a_n) \sigma^x \\ &\quad - \sum_n \omega_n \alpha_n(t) \alpha_n^*(t) + \sum_n g_n (\alpha_n(t) + \alpha_n^*(t)) \sigma^x, \end{aligned} \quad (6)$$

where $\sum_n g_n (\alpha_n(t) + \alpha_n^*(t))$ can be replaced by the interaction of the classical field at the emitter position with the emitter dipole, $-\mu \mathcal{E}(t)$, while $\sum_n \omega_n \alpha_n(t) \alpha_n^*(t) = \sum_n \omega_n |\alpha_n(0)|^2$ just corresponds to a constant energy shift that can be neglected. In the following, we thus use $\mathcal{H} = H_d - \mu \mathcal{E}(t) \sigma^x$, i.e.,

$$\mathcal{H} = \sum_n \omega_n a_n^\dagger a_n + \frac{\Omega_0}{2} \sigma^z + \sum_n g_n (a_n^\dagger + a_n) \sigma^x - \mu \mathcal{E}(t) \sigma^x, \quad (7)$$

as the effective Hamiltonian and take the initial state as the vacuum state with the emitter in its ground state.⁶¹ However, it is important to remember that EM field observables are also transformed according to

$$\langle \psi | O | \psi \rangle = \langle \psi' | T(t) O T^\dagger(t) | \psi' \rangle, \quad (8)$$

such that, e.g., $\langle \psi | a_n | \psi \rangle = \langle \psi' | a_n + \alpha_n(t) | \psi' \rangle$. This takes into account the ‘‘quantum’’ field generated by the laser–emitter interaction interferes with the classical pulse propagating through the structure and ensures a correct description of absorption of the pulse, coherent scattering, and similar effects. We note that the above properties imply that within this framework, the action of any incoming laser pulse on the *full* emitter–cavity system can be described purely by the action of the medium-enhanced classical electric field driving the emitter, with no additional explicit driving of any EM modes. This is in contrast to, e.g., input–output theory, where the EM field is split into modes inside the cavity and free-space modes outside, and external driving thus affects the cavity modes. It should be stressed in this context that $\mathcal{E}(t)$ is the field obtained at the position of the emitter after propagation of the external laser pulse through the cavity structure, i.e., it contains any field enhancement and temporal distortion induced by the cavity. In practice, it is thus most straightforward to employ classical EM simulations to calculate the electric field J reaching the emitter for a given input pulse and cavity structure.

A. Heisenberg equations of motion

The evolution of any expectation value $\langle O \rangle = \langle \psi' | O | \psi' \rangle$ can be described by the Heisenberg equation of motion,

$$\partial_t \langle O \rangle = i \langle [\mathcal{H}, O] \rangle. \quad (9)$$

In general, the time derivative of products of N operators $\langle A_1 A_2 \dots A_N \rangle$ includes the contribution of $N + 1$ operators $\langle A_1 A_2 \dots A_N A_{N+1} \rangle$ due to the bilinear matter–field coupling in Eq. (7), so one obtains an infinite set of equations that describe the system. Truncating these expansions and, thus, neglecting some contributions leads to a closed set of equations. This can be done in a systematic way using the cumulant expansion (also known as cluster expansion^{54,55} or truncated BBGKY hierarchy⁵⁸). The cumulant expansion method expresses an expectation value as sums and products of expectation values of a smaller number

of operators and their correlations and itself does not imply any approximation. However, it then allows us to systematically discard only high-order correlations and not just high-order expectation values.

As an aside, we note that the meaning of “order of the approximation” depends on which set of operators is used to represent the system. For example, we use σ^x , σ^y , and σ^z as the “fundamental” operators, but it would be equally possible to use only σ^x and σ^y (or more conventionally $\sigma^\pm = \frac{1}{2}\sigma^x \pm \frac{i}{2}\sigma^y$) as $\sigma^z = \sigma^+ \sigma^- - \sigma^- \sigma^+ = 2\sigma^+ \sigma^- - 1$. Similarly, we only use a_n and a_n^\dagger , but it would be equally possible to add the number operator N_n and, thus, obtain photonic populations at lower orders. The convention we use is chosen because of the direct connection to Maxwell–Bloch and other mean-field approximations, where the population of the two-level system is considered explicitly within the set of equations, while only the coherent part of the EM fields is treated.

In addition to the different levels of approximation for the dynamics obtained by truncating the systems at various orders, it should be noted that the order of the expansion needed to describe the system also depends on the expectation values of interest. For example, the second-order correlation function $g^{(2)}(0)$ contains expectation values of products of four operators and is exactly equal to unity within the mean-field approximation.

We next show the set of equations obtained in our system at various orders and discuss possible strategies for truncation. Some of these equations have been obtained by using the QuantumAlgebra.jl package⁶² for symbolic calculation of quantum operator expressions.

The set of equations that arise from applying Eq. (9) to single operators (i.e., at first order) are

$$\partial_t \langle a_n \rangle = -i\omega_n \langle a_n \rangle - ig_n \langle \sigma^x \rangle, \quad (10a)$$

$$\partial_t \langle \sigma^x \rangle = -i\Omega_0 \langle \sigma^y \rangle, \quad (10b)$$

$$\partial_t \langle \sigma^y \rangle = \Omega_0 \langle \sigma^x \rangle - 2 \sum_n g_n \langle a_n^\dagger \sigma^z \rangle + 2\mu E(t) \langle \sigma^z \rangle, \quad (10c)$$

$$\partial_t \langle \sigma^z \rangle = 2 \sum_n g_n \langle a_n^\dagger \sigma^y \rangle - 2\mu E(t) \langle \sigma^y \rangle. \quad (10d)$$

Within the cumulant expansion, the expectation value of a product of operators is expressed as $\langle ab \rangle = \langle a \rangle \langle b \rangle + \langle ab \rangle_C$, where $\langle ab \rangle_C$ is the correlation between a and b . The mean-field approximation consists in already neglecting all two-operator correlations, i.e., to assume $\langle ab \rangle_C \simeq 0$. If this approximation is made, Eqs. (10) form a closed set that can be propagated in time.

At the next order of approximation, correlations up to second order are taken into account. Then, the Heisenberg equations of motion that arise are

$$\partial_t \langle a_n^\dagger \sigma^x \rangle = i\omega_n \langle a_n^\dagger \sigma^x \rangle - \Omega_0 \langle a_n^\dagger \sigma^y \rangle + ig_n, \quad (11a)$$

$$\begin{aligned} \partial_t \langle a_n^\dagger \sigma^y \rangle &= i\omega_n \langle a_n^\dagger \sigma^y \rangle + \Omega_0 \langle a_n^\dagger \sigma^x \rangle - g_n \langle \sigma^z \rangle - 2 \sum_m g_m \\ &\times \left(\langle a_n^\dagger a_m^\dagger \sigma^z \rangle + \langle a_n^\dagger a_m \sigma^z \rangle \right) + 2\mu \mathcal{E}(t) \langle a_n^\dagger \sigma^z \rangle, \end{aligned} \quad (11b)$$

$$\begin{aligned} \partial_t \langle a_n^\dagger \sigma^z \rangle &= i\omega_n \langle a_n^\dagger \sigma^z \rangle + g_n \langle \sigma^y \rangle + 2 \sum_m g_m \\ &\times \left(\langle a_n^\dagger a_m^\dagger \sigma^y \rangle + \langle a_n^\dagger a_m \sigma^y \rangle \right) - 2\mu \mathcal{E}(t) \langle a_n^\dagger \sigma^y \rangle, \end{aligned} \quad (11c)$$

$$\partial_t \langle a_n^\dagger a_m \rangle = i(\omega_n - \omega_m) \langle a_n^\dagger a_m \rangle + ig_n \langle a_m \sigma^x \rangle - ig_m \langle a_n^\dagger \sigma^x \rangle, \quad (11d)$$

$$\partial_t \langle a_n^\dagger a_m^\dagger \rangle = i(\omega_n + \omega_m) \langle a_n^\dagger a_m^\dagger \rangle + ig_n \langle a_m^\dagger \sigma^x \rangle + ig_m \langle a_n^\dagger \sigma^x \rangle. \quad (11e)$$

Since $\langle a_n \sigma^j \rangle = \langle a_n^\dagger \sigma^j \rangle^*$ and $\langle a_n^\dagger a_m^\dagger \rangle = \langle a_m a_n \rangle^*$, Eqs. (11) enough to describe all combinations of two operators. In the cumulant expansion, we re-express $\langle abc \rangle = \langle a \rangle \langle b \rangle \langle c \rangle + \langle a \rangle \langle bc \rangle_C + \langle b \rangle \langle ac \rangle_C + \langle c \rangle \langle ab \rangle_C + \langle abc \rangle_C$. For completeness, we here give the equations of motion of the correlations explicitly,

$$\partial_t \langle a_n^\dagger \sigma^x \rangle_C = i\omega_n \langle a_n^\dagger \sigma^x \rangle_C - \Omega_0 \langle a_n^\dagger \sigma^y \rangle_C + ig_n (1 - \langle \sigma^x \rangle \langle \sigma^x \rangle), \quad (12a)$$

$$\begin{aligned} \partial_t \langle a_n^\dagger \sigma^y \rangle_C &= i\omega_n \langle a_n^\dagger \sigma^y \rangle_C + \Omega_0 \langle a_n^\dagger \sigma^x \rangle_C - g_n (\langle \sigma^z \rangle - i \langle \sigma^x \rangle \langle \sigma^y \rangle) \\ &+ 2\mu \mathcal{E}(t) \langle a_n^\dagger \sigma^z \rangle_C - 2 \sum_m g_m \left(\langle a_m^\dagger \rangle \langle a_n^\dagger \sigma^z \rangle_C \right. \\ &+ \langle a_m \rangle \langle a_n^\dagger \sigma^z \rangle_C + \langle \sigma^z \rangle \langle a_n^\dagger a_m^\dagger \rangle_C + \langle \sigma^z \rangle \langle a_n^\dagger a_m \rangle_C \\ &+ \left. \langle a_n^\dagger a_m^\dagger \sigma^z \rangle_C + \langle a_n^\dagger a_m \sigma^z \rangle_C \right), \end{aligned} \quad (12b)$$

$$\begin{aligned} \partial_t \langle a_n^\dagger \sigma^z \rangle_C &= i\omega_n \langle a_n^\dagger \sigma^z \rangle_C + g_n (\langle \sigma^y \rangle - i \langle \sigma^x \rangle \langle \sigma^z \rangle) \\ &- 2\mu \mathcal{E}(t) \langle a_n^\dagger \sigma^y \rangle_C + 2 \sum_m g_m \left(\langle a_m^\dagger \rangle \langle a_n^\dagger \sigma^z \rangle_C \right. \\ &+ \langle a_m \rangle \langle a_n^\dagger \sigma^z \rangle_C + \langle \sigma^y \rangle \langle a_n^\dagger a_m^\dagger \rangle_C + \langle \sigma^y \rangle \langle a_n^\dagger a_m \rangle_C \\ &+ \left. \langle a_n^\dagger a_m^\dagger \sigma^y \rangle_C + \langle a_n^\dagger a_m \sigma^y \rangle_C \right), \end{aligned} \quad (12c)$$

$$\partial_t \langle a_n^\dagger a_m \rangle_C = i(\omega_n - \omega_m) \langle a_n^\dagger a_m \rangle_C + ig_n \langle a_m \sigma^x \rangle_C - ig_m \langle a_n^\dagger \sigma^x \rangle_C, \quad (12d)$$

$$\partial_t \langle a_n^\dagger a_m^\dagger \rangle_C = i(\omega_n + \omega_m) \langle a_n^\dagger a_m^\dagger \rangle_C + ig_n \langle a_m^\dagger \sigma^x \rangle_C + ig_m \langle a_n^\dagger \sigma^x \rangle_C. \quad (12e)$$

The cumulant expansion provides a systematic approach to approximate the true solution by neglecting higher-order correlations between operators. *A priori*, one could assume that it is always a better approximation to neglect a correlation $\langle A_1 \dots A_n \rangle_C$ than the corresponding expectation value $\langle A_1 \dots A_n \rangle$ directly. However, as we will see later, this assumption is not always correct and whether to neglect correlations or expectation values is a better approximation depends on the physical system and concrete situation.

We also mention that while Eqs. (11) describing the expectation values are linear, the corresponding correlation expansion, Eqs. (12) correspond to a nonlinear system depending on products of the state variables (expectation values and correlations). These nonlinearities make the obtained set of equations numerically more unstable.

In Eqs. (12), no approximations have been made as no correlations have been neglected yet. To obtain a closed set of equations that may allow the description of the time evolution of the system, some correlations have to be neglected again. The second-order cumulant expansion approximation means to neglect the correlations of three of more operators ($\langle abc \rangle_C \simeq 0$) so that the set of Eqs. (10) and (12) are enough to find a solution. The same procedure as above can be followed to obtain the equations up to third order, i.e., neglecting correlations of four or more operators (for reference, the required cumulant expansion is given in Appendix A).

The third-order expectation values needed to describe the third order completely are $\langle a_n^\dagger a_m \sigma^{x,y,z} \rangle$, $\langle a_n^\dagger a_m^\dagger \sigma^{x,y,z} \rangle$, $\langle a_n^\dagger a_m^\dagger a_l \rangle$, and $\langle a_n^\dagger a_m^\dagger a_l^\dagger \rangle$, with their explicit equations of motion given in Appendix B. The equations for the correlations are not written, but it is straightforward to derive them from the equations of motion of the expectation values.

The numerical implementation of the equations is performed within the Julia programming language.⁶³ The code runs on graphical processing units (GPUs), which provides a significant speedup (≈ 20 for our available setup) over the central processing unit (CPU) variant of the same code. For the time propagation, we rely on the DifferentialEquations.jl package.⁶⁴

III. RESULTS

A. Free space dynamics

The spectral density of an emitter in free space is

$$J(\omega) = \hbar \omega^3 \frac{|\mu|^2}{6\pi\epsilon_0 c^3}. \quad (13)$$

Discretizing this spectral density with frequency spacing $\Delta\omega$ is equivalent to describing an emitter in center of a spherical box of radius $R = \pi c/\Delta\omega$,⁶⁵ where c is the speed of light in vacuum. As a first example, we will treat spontaneous emission from an initially excited emitter, i.e., the classical Wigner–Weisskopf problem.⁶⁶ If time propagation is performed over too long times ($\approx 2R/c = 2\pi/\Delta\omega$, the time that it takes the photon to propagate from the emitter to the boundary of the sphere and back), artificial reflections of the emitted photons from the boundaries of the sphere are obtained and interact again with the emitter. As the lifetime of typical emitters (atoms, molecules, quantum dots) is on the scale of nanoseconds, an accurate description would require a very small frequency spacing and, thus, a very large box, and additionally, propagation over very long times. To avoid this, we instead set the emitter dipole moment to the unrealistically large value of $\mu = 2565$ D, for which the spontaneous emission lifetime at the emitter frequency of $\Omega_0 = 2.72$ eV is given by $\tau \approx 46$ fs. We choose $N = 400$ photonic modes on a regular grid in frequency from 0 eV to 5.44 eV. For these parameters, spontaneous emission takes place within a time shorter than $2R/c$.

The spontaneous emission dynamics of an initially excited single emitter in free space is shown in Fig. 1, which shows the excited-state population of the emitter as a function of time, calculated using three different numerical methods: Perturbative Wigner–Weisskopf (WW) theory, which simply predicts exponential decay with rate $\gamma = J(\Omega_0)$, mean-field (MF), and second-order cumulant expansion (2). As is well-known, the mean-field approximation does not predict any spontaneous emission. This is because this phenomenon is due to the interaction of the emitter with the vacuum fluctuations $\langle a_n^\dagger a_m \rangle$ and the mean-field approximation neglects all the expectation values of two or more operators. Since $\langle a_n \rangle = \langle \sigma^x \rangle = \langle \sigma^y \rangle = 0$ at $t = 0$ and no external electric field affects the system, no dynamics are predicted. Going beyond mean-field is thus essential to describe spontaneous emission.^{27,67} On the other hand, the second-order cumulant expansion (and all higher-order approaches, not shown) already perfectly describes the free-space spontaneous decay of $\langle \sigma^+ \sigma^- \rangle$ due to the vacuum fluctuations.

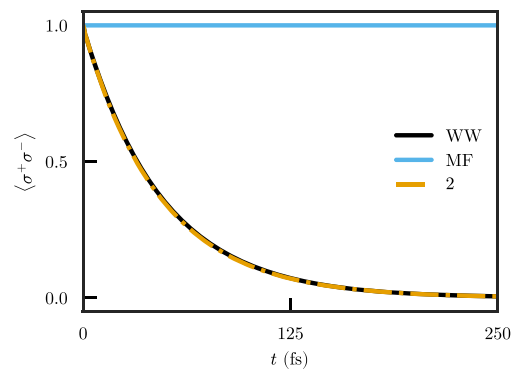


FIG. 1. Excited-state population of the emitter in time in free space. Comparison between Wigner–Weisskopf approximation (silver line), mean-field (light green line), and second-order approximation (medium green dashed–dotted line).

We next consider an emitter initially in its ground state, $\langle \sigma^+ \sigma^- \rangle(t = 0) = 0$ under pumping by a classical electric field $\mathcal{E}(t)$. We use a short Gaussian pulse in resonance with the emitter transition frequency, $\mathcal{E}(t) = \mathcal{E}_0 e^{-(t-t_0)^2/2T^2} \sin(\Omega_0 t)$. In order to describe a more realistic system, the dipole moment of the emitter is set to $\mu = 2.56$ D, corresponding to a spontaneous emission lifetime in free space of $\tau \approx 46$ ns. The pulse parameters are $t_0 = 77.76$ fs and $T = 24.20$ fs. We now compare the mean-field and second-order approaches with a semi-classical approximation in which no quantized light modes are present at all, and the two-level system interacts with the EM field via the equations,

$$\frac{\partial}{\partial t} \begin{pmatrix} C_g \\ C_e \end{pmatrix} = -i \begin{pmatrix} 0 & -\mu \cdot \mathcal{E}(t) \\ -\mu \cdot \mathcal{E}(t) & \Omega_0 \end{pmatrix} \cdot \begin{pmatrix} C_g \\ C_e \end{pmatrix}, \quad (14)$$

where C_g and C_e are the ground-state and excited-state amplitudes, respectively. The peak amplitudes of the electric field we consider are $\mathcal{E}_0 = 0.051$ V/Å [Fig. 2(a)], $\mathcal{E}_0 = 0.257$ V/Å [Fig. 2(b)], and $\mathcal{E}_0 = 0.514$ V/Å [Fig. 2(c)]. For the weakest driving we consider that the system is already in the nonlinear regime but the electric field is weak enough so that no Rabi oscillations are seen in the atom dynamics [subplot (a)], while the two stronger fields lead to a strongly nonlinear response with driven Rabi oscillations [subplots (b) and (c)]. In this case, the coupling to the free-space modes is so weak that they are not expected to have any influence on the dynamics, and this is, indeed, observed in Fig. 2. All three approaches (semi-classical, mean-field, and second order) accurately describe the emitter dynamics, and correlations between the photonic modes and the emitter can be neglected. After the end of the pulse, the spontaneous decay (with lifetime $\tau \approx 46$ ns) is so slow that it is not noticeable over the time scales we investigate although it would show up eventually for longer propagation times for the second-order approach.

B. Cavity

We next consider a spectral density that represents a single lossy cavity mode. This is achieved using a Lorentzian frequency dependence,

$$J(\omega) = \frac{g^2}{\pi} \frac{\gamma/2}{(\omega - \omega_c)^2 + (\gamma/2)^2}. \quad (15)$$

The dynamics predicted using this spectral density is mathematically equivalent to those of the Lindblad master equation

$$\partial_t \rho = -i[H_R, \rho] + \gamma \mathcal{L}_a[\rho], \quad (16)$$

where H_R is the Rabi Hamiltonian,

$$H_R = \frac{\Omega_0}{2} \sigma^z + \omega_c a^\dagger a + g(a + a^\dagger) \sigma^x, \quad (17)$$

for interaction of a single emitter with a single quantized mode, while $\mathcal{L}_a[\rho] = a\rho a^\dagger - \frac{1}{2}\{a^\dagger a, \rho\}$ is the Lindblad operator that describes the cavity losses. The effective coupling $g = \mu E_{1ph}$ is determined by the amplitude of the Lorentzian spectral density, the effective losses are given by its width γ , and the frequency of the photonic mode is the resonance frequency ω_c of the Lorentzian.^{22,44}

The emitter and cavity frequencies are both set to $\Omega_0 = \omega_c = 2.72$ eV. We choose a bandwidth of $\gamma = 0.027$ eV (Q-factor $Q = \omega_c/\gamma = 100$) and will consider various coupling amplitudes g . The number of modes considered is $N = 400$, and the frequencies

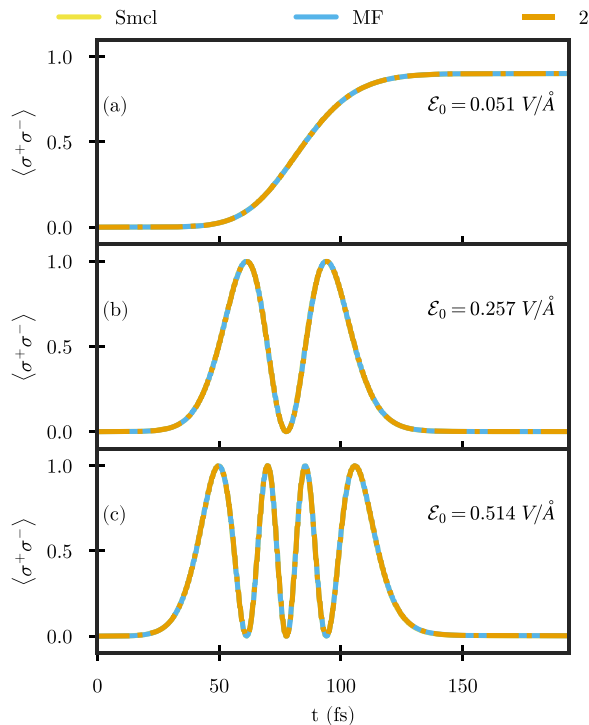


FIG. 2. Excited-state population of a single emitter in free space under driving by a short Gaussian pulse. The peak electric field amplitude increases from (a) to (c) and is shown in each subplot. Comparison between semi-classical approximation (yellow line), mean-field (light green line), and second-order approximation (dotted-dashed medium green line). All lines are indistinguishable for this case.

are taken from $\omega_{\min} = 2.04$ eV to $\omega_{\max} = 3.40$ eV (grid spacing $\Delta\omega = 3.4$ meV), so the range is wide enough and the number of modes is big enough to represent the Lorentzian spectral density.

The emitter is initially in its excited state $\langle \sigma^+ \sigma^- \rangle(t=0) = 1$ and evolves freely in the cavity, without any external electric field. While we do not employ the rotating wave approximation (RWA), which consists in neglecting the counter-rotating terms $a_n^\dagger \sigma^+$ and $a_n \sigma^-$ in the Hamiltonian, it is approximately fulfilled for the coupling values we choose here. Within the RWA, the number of excitations $\sigma^+ \sigma^- + \sum_n a_n^\dagger a_n$ is conserved. In Fig. 3, the evolution of the emitter population is shown for a coupling strength of $g = 0.008$ eV, for which the system is already close to the strong-coupling regime ($4g > \gamma$).⁶⁸ In contrast to the free-space case, the second-order approximation [shown in Fig. 3(a)] now starts to show some differences with respect to exact solution obtained with the Rabi model, with the population even reaching nonphysical values, $\langle \sigma^+ \sigma^- \rangle < 0$. This implies that some third-order terms are required to obtain the correct dynamics, but it is not clear *a priori* which additional terms have to be included. We thus compare different extensions of the second-order expansion by successively adding higher-order terms. In the first one, the second-order set of Eqs. (10) and (12) is used, but in Eq. (12b), the term $\langle a_n^\dagger a_m \sigma^z \rangle_C$ and its dynamics are not neglected. We denote this second-order approximation with a correction by “2+1a” in the following. The importance of including the particular third-order term has been previously pointed out in the literature⁵⁶ and is due to it being the third-order correction with the largest value. Taking into account that, to a good approximation, the state during the dynamics is described by a single excitation, $|\psi\rangle \approx (\alpha\sigma^+ + \sum_n \beta_n a_n^\dagger)|0\rangle$, we can easily see this by inspecting the cumulant expansion of the third-order expectation values. For $\langle a_n^\dagger a_m \sigma^z \rangle$, this gives

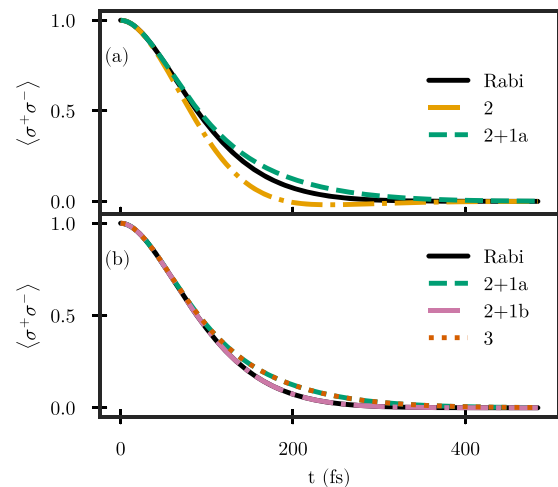


FIG. 3. Excited-state population for an initially excited emitter in a cavity for coupling $g = 0.008$ eV. (a) Comparison between the exact Rabi model solution (purple line), 2nd order (medium green line) and 2+1a (dashed dark green line) approximation. (b) Comparison between the Rabi solution (purple line), 2+1a approximation (dashed dark green line), 2+1b approximation (dashed dotted blue line), and 3rd order (dotted red line).

$$\begin{aligned} \langle a_n^\dagger a_m \sigma^z \rangle &= \langle a_n^\dagger \rangle \langle a_m \rangle \langle \sigma^z \rangle + \langle a_n^\dagger \rangle \langle a_m \sigma^z \rangle_C + \langle a_m \rangle \langle a_n^\dagger \sigma^z \rangle_C \\ &+ \langle \sigma^z \rangle \langle a_n^\dagger a_m \rangle_C + \langle a_n^\dagger a_m \sigma^z \rangle_C. \end{aligned} \quad (18)$$

The first three terms are negligible since $\langle a_n \rangle \approx 0$, but the product $\langle \sigma^z \rangle \langle a_n^\dagger a_m \rangle_C$ is non-negligible since both the emitter and photonic mode populations are nonzero. At the same time, it does not approximate the value of $\langle a_n^\dagger a_m \sigma^z \rangle$ well so that the correlation $\langle a_n^\dagger a_m \sigma^z \rangle_C$ is necessarily non-zero. In contrast, the expansion of $\langle a_n^\dagger a_m \sigma^y \rangle$ gives

$$\begin{aligned} \langle a_n^\dagger a_m \sigma^y \rangle &= \langle a_n^\dagger \rangle \langle a_m \rangle \langle \sigma^y \rangle + \langle a_n^\dagger \rangle \langle a_m \sigma^y \rangle_C + \langle a_m \rangle \langle a_n^\dagger \sigma^y \rangle_C \\ &+ \langle \sigma^y \rangle \langle a_n^\dagger a_m \rangle_C + \langle a_n^\dagger a_m \sigma^y \rangle_C. \end{aligned} \quad (19)$$

Here, all the product terms contain at least one negligible value as $\langle \sigma^y \rangle \approx 0$, while $\langle a_n^\dagger a_m \sigma^y \rangle$ is also zero for the single-excitation state given above. This implies that the correlation $\langle a_n^\dagger a_m \sigma^y \rangle_C$ is in turn also negligible.

In the equation of motion of the new term $\langle a_n^\dagger a_m \sigma^z \rangle$, fourth-order expectation values appear; see Eq. (B1c) in Appendix B. Performing the cumulant expansion on these and neglecting the fourth-order correlation, it is easy to see that only third-order correlations that are neglected in the other equations appear, and by consistency, these terms are approximated up to the second order as well, leading to Eq. (B2).

As seen in Fig. 3(a), the dynamics of the emitter within the 2+1a approximation are changed, with the population never reaching negative values. However, it still does not agree with the exact solution provided by the Rabi model and is now overestimated. Inspection of the equation of motion for $\langle a_n^\dagger a_m \sigma^z \rangle$ [Eq. (B1c)] shows that this contains fourth-order terms that involve two photonic creation or annihilation operators. For the current dynamics, where to a good approximation only one excitation is present in the system, these fourth-order expectation values are thus approximately zero. Within the 2+1a approximation, they are, however, represented by products of non-negligible second-order correlations that have non-zero values. It is then possible to improve the approximation by not performing a cumulant expansion on the fourth-order terms in Eq. (B1c), but by neglecting them directly. We are going to refer to this approximation as “2+1b.” When using it [shown in Fig. 3(b)], the emission dynamics are now correctly obtained.

Finally, we also perform the full third-order expansion, with the cumulant expansion performed on all expectation values and fourth-order correlations being neglected. The third-order approximation [also shown in Fig. 3(b)] provides identical results as the 2+1a approach, proving that, indeed, all third-order correlations apart from $\langle a_n^\dagger a_m \sigma^z \rangle_C$ can be neglected. However, for good agreement with the exact results, the same correction as in the 2+1b approach would have to be performed or alternatively the full expansion would have to be performed up to at least fourth order.

We note here that numerically both approximations 2+1a and 2+1b are only slightly more costly than the second-order expansion since the added term $\langle a_n^\dagger a_m \sigma^z \rangle_C$ only contains two continuum indices n and m . In contrast, the full third-order expansion contains terms of the form $\langle a_n a_m a_o \rangle_C$ with three continuum mode indices

(represented by $N \times N \times N$ arrays) and is thus significantly more expensive to implement.

We now increase the coupling strength to $g = 0.024$ eV, squarely in the strong-coupling regime where vacuum Rabi oscillations are expected, and study the emitter dynamics as shown in Fig. 4. All the previous approximations are compared again. The nonphysical values that the population takes in the second-order approximation are more evident when the coupling increases although the Rabi oscillation frequency is reproduced well. For the 2+1a approximation, which again gives identical results as the full third-order expansion, this does not hold. This is because the correlations that appear in the equation of motion of $\langle a_n^\dagger a_m \sigma^z \rangle_C$ interact via the coupling, so if the coupling increases, the modifications produced by the spurious correlations also increase. The correction 2+1b, i.e., enforcing the fourth-order expectation value in Eq. (B1c) to be zero, again predicts the exact dynamics accurately since the system remains in the single-excitation subspace even in strong coupling. These conclusions are essentially unchanged even when increasing the coupling to $g = 0.086$ eV, shown in Fig. 5.

We next compare the same physical system and the same approximations, but now not for the case of spontaneous emission and vacuum Rabi oscillations, but for the emitter initially in its ground state, $\langle \sigma^+ \sigma^- \rangle(t=0) = 0$, and driven by an incoming classical electric field. Two different pulses are considered. First, we take the same short Gaussian pulse considered in free space $\mathcal{E}(t) = \mathcal{E}_0 e^{-(t-t_0)^2/2T^2} \sin(\Omega_0 t)$ (assumed to be the pulse reaching the emitter after enhancement and distortion by propagating through the cavity structure). In the second case, we choose an electric field that smoothly turns on and then remains at a stationary intensity indefinitely, $\mathcal{E}(t) = \mathcal{E}_0 \sin(\Omega_0 t) (\theta(t_0 - t) e^{-(t-t_0)^2/2T^2} + \theta(t - t_0))$, where $\theta(t)$ is the Heaviside theta function, allowing to study if and how a steady state is reached in the time propagation. In both cases, the pump laser frequency is in resonance with the emitter and cavity resonances.

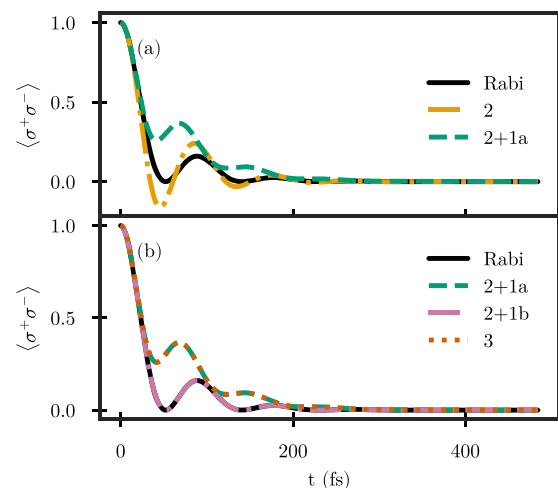


FIG. 4. Excited-state population of an initially excited emitter in a cavity in the strong-coupling regime, with $g = 0.024$ eV. Subplots and lines like in Fig. 3.

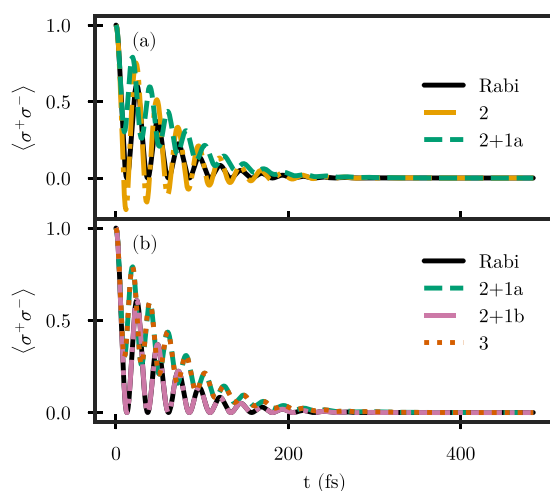


FIG. 5. Excited-state population of an initially excited emitter in a cavity in the strong-coupling regime, with $g = 0.086$ eV. Subplots and lines like in Figs. 3 and 4.

We first again use the cavity with the weakest light–matter coupling ($g = 0.008$ eV). The emitter population dynamics when a Gaussian pulse excites the system is shown in Fig. 6, while the steady-state pulse is shown in Fig. 7. In both figures, we compare the same approximations as above with the exact Rabi model solution. The amplitudes of the electric field interacting with the emitter are the same as in free space, given by $\mu\mathcal{E}_0 = 0.026$ eV [subplots (a) and (b)], $\mu\mathcal{E}_0 = 0.132$ eV [subplots (c) and (d)], and $\mu\mathcal{E}_0 = 0.263$ eV [subplots (e) and (f)].

In contrast to the free-space case, the quantum effects due to fluctuations, such as spontaneous emission, are not negligible here, and the mean-field approximation [shown in subplots (a), (c), and (e)] fails to capture the dynamics as it can only represent the coherent contribution to the light–matter interaction.²⁷ In the short-pulse case [Fig. 6], this is mostly seen in the dynamics after the pulse but is also reflected in Rabi oscillations during the pulses with bigger amplitudes than the ones predicted by the exact solution. Still, the mean-field approximation does give a qualitatively correct prediction of the behavior for the short-pulse case (Fig. 6). In the case of a long pulse (Fig. 7), the initial driven oscillations are well-described but, as there is no coupling between the fluctuations and the emitter, no steady state is achieved and the population keeps oscillating indefinitely. If the decay rate of the emitter is known, incoherent contributions to the emitter dynamics can be incorporated *ad hoc* using phenomenological decay constants.⁶⁹ However, obtaining these constants is not always easy and is only straightforward in the weak-coupling regime where the light and matter degrees of freedom are not mixed. In those case, the validity and simplicity of the mean-field approximation makes it a common tool in describing a wide range of systems pumped by lasers.^{22,70}

The second-order approximation [subplots (a), (c), and (e)] is sufficient to describe the dynamics in this regime. When the amplitude of the electric field is $\mathcal{E}_0 = 0.051$ V/Å and the pulse is short [Fig. 6(a)], the dynamics predicted by this approximation are much more similar to the Rabi solution as incoherent contributions are

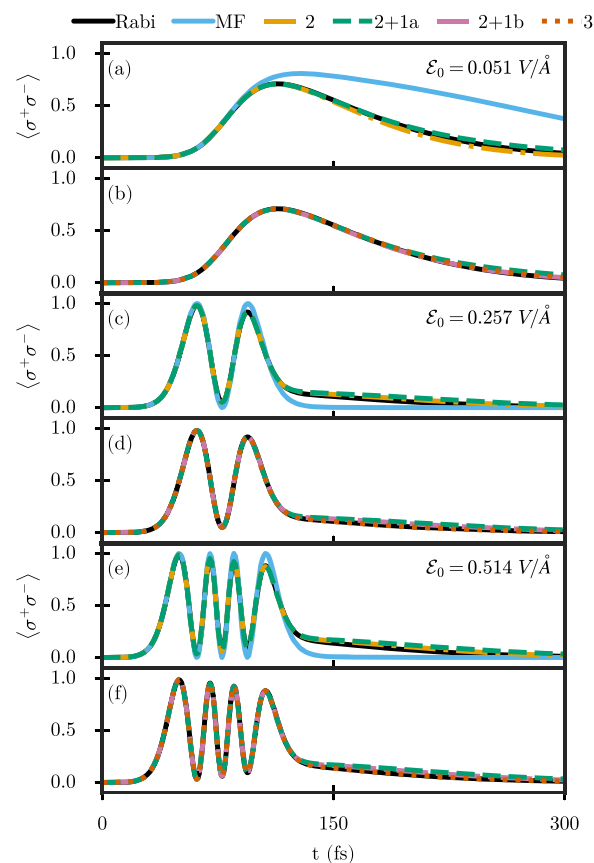


FIG. 6. Excited-state population for an emitter initially in the ground state within a cavity with $g = 0.008$ eV, driven by a short classical electric field pulse (see text for details), for three different peak amplitudes as indicated in the subplots. (a), (c), and (e) Comparison between the Rabi solution (purple line), mean-field (light green line), 2nd order (medium green dashed–dotted line), and 2+1a approximation (dark green dashed line). (b), (d), and (f) Comparison between Rabi solution (purple line), 2+1a approach (dashed dark green line), 2+1b approach (dashed dotted blue line), and 3rd order (dotted red line).

taken into account via the second-order terms. For a long pulse [Fig. 7(a)], the oscillations are not accurately described, neither in shape nor in amplitude, but it does give a qualitative prediction and the steady state is predicted quantitatively. Making the correction 2+1a to the second order changes the dynamics only slightly. The extra correlations included by this correction lead to a decrease in the oscillation amplitude, but the qualitative description is maintained. Finally, enforcing the fourth order expectation values to be zero via the correction 2+1b (subplot b), i.e., enforcing the system to have only one excitation, hardly changes the prediction of the emitter dynamics.

If the driving electric field is more intense [subplots (c), (d), (e), and (f)], the second-order approximation [subplots (c) and (e)] gives a correct description of the shape of the Rabi oscillations, but their amplitude is underestimated. Approximations 2+1a and 2+1b [subplots (d) and (f)] do not show any difference with respect to the “bare” second order. Thus, correlations that change the description

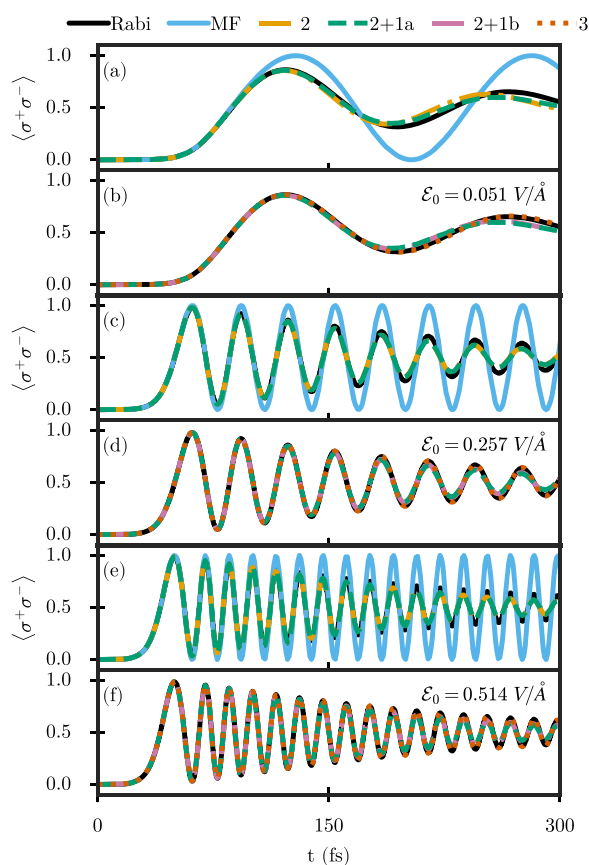


FIG. 7. Same as Fig. 6, but for a semi-infinite driving pulse with constant amplitude after a smooth turn-on (see text for details).

of the dynamics completely in the case of spontaneous emission do not matter much in the more classical case of driving by a strong laser pulse. Finally, the third-order approximation is shown in subplots (b), (d), and (f). Adding all the third-order correlations sufficiently modifies the dynamics to achieve an accurate prediction in good agreement with the Rabi model.

From the results in Figs. 6 and 7, we can conclude that when the light–matter coupling is not too strong, the second-order correlations are the most important and, in general, this order of approximation is enough to describe the main characteristics of the solution. If a more quantitative description is required, the third-order approximation achieves almost perfect agreement with the exact dynamics.

The results obtained when again increasing the light–matter coupling strength to $g = 0.024$ eV are shown in Fig. 8 for the Gaussian pulse and in Fig. 9 for the semi-infinite pulse, with the same driving pulses as in the previous case. When the amplitude of the electric field is $\mathcal{E}_0 = 0.051$ V/Å [subplots (a) and (b)], its magnitude is comparable to the coupling strength. The mean-field approximation [subplot (a)] then overestimates the population oscillations for both classical fields. This continues for more intense driving fields [subplots (c) and (e)]. As mentioned above, while the

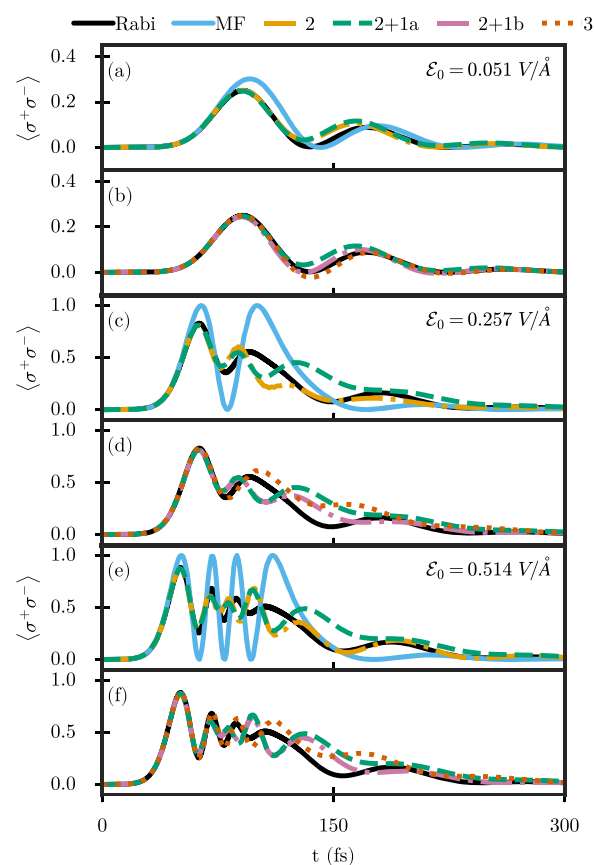


FIG. 8. Same as Fig. 6, but for emitter-cavity coupling of $g = 0.024$ eV.

mean-field approximation cannot reproduce spontaneous decay by itself, adding phenomenological decay constants to the mean-field equations can be used to achieve reasonable descriptions of the strong-coupling regime for intense classical fields.⁷¹ However, doing so means that the photons emitted due to field fluctuations are not represented so that, e.g., the spontaneous emission from polaritonic states⁷² could not be monitored in the emitted field.

Compared to the mean-field approach, the second-order approximation better predicts both the short-time dynamics as well as the steady-state limit for the semi-infinite pulse for the weak driving amplitude $\mathcal{E}_0 = 0.051$ V/Å, but slightly overestimates the population at intermediate times. This overall picture also applies for the stronger driving strengths [subplots (c)–(f)]. The corrections 2+1a and 2+1b somewhat improve upon the bare second-order calculation, with 2+1a working slightly better for the semi-infinite pulses (Fig. 9) and 2+1b working slightly better under short-pulse driving (Fig. 8). Finally, as could be expected, the third-order approximation improves the results for both the short and semi-infinite pulses. In particular, it perfectly reproduces the exact results during the first few Rabi oscillations and converges to the correct steady-state limit under long-pulse driving faster than the lower-order expansions. However, even the third-order expansion does not fully reproduce the dynamics at intermediate times, where decoherence starts

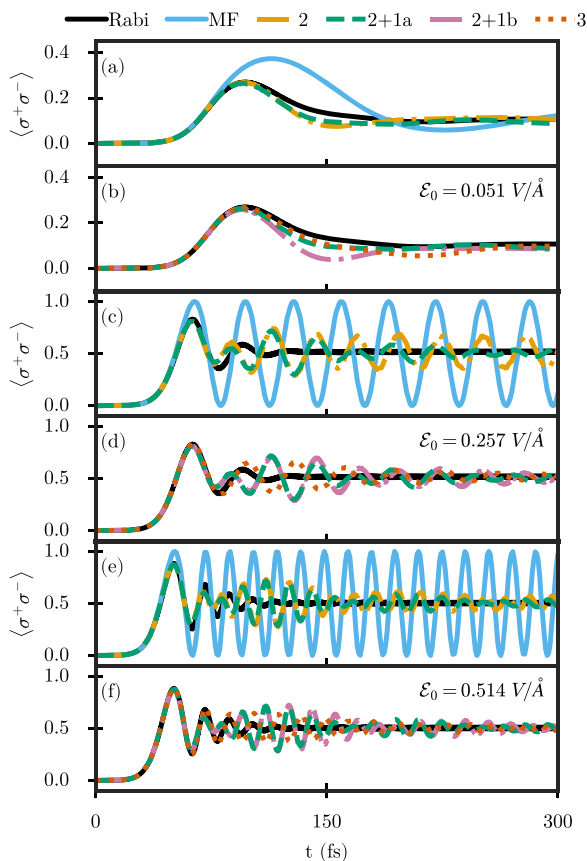


FIG. 9. Same as Fig. 8, but for a semi-infinite driving pulse with constant amplitude after a smooth turn-on.

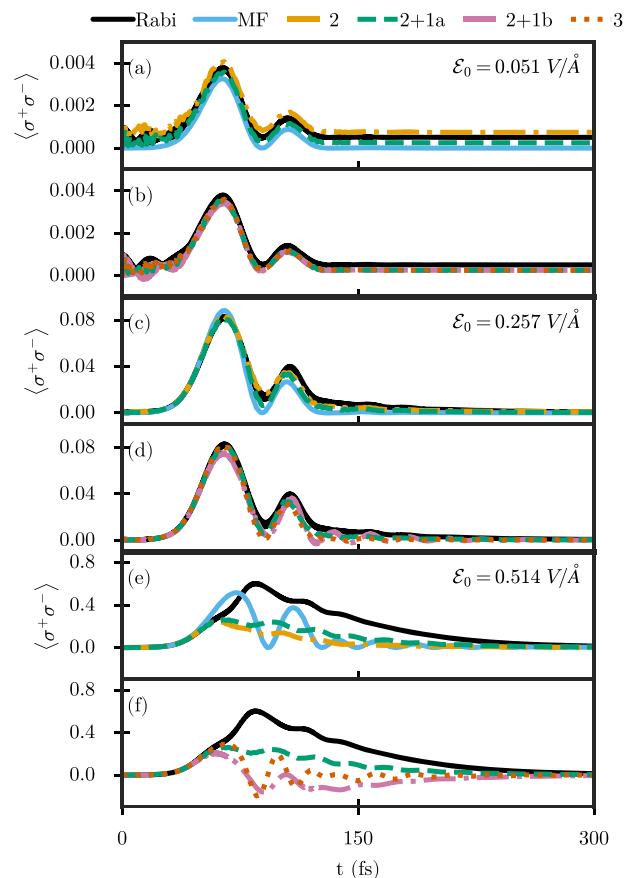


FIG. 10. Same as Fig. 6, but for emitter-cavity coupling of $g = 0.086$ eV.

to set in and induces corrections to the coherent dynamics, which are reflected in higher-order light-matter correlations at intermediate times. At longer times, where the system becomes mostly incoherent, the light-matter correlations are again well-described by lower-order expansions, and the steady state is thus well-represented within the third-order and even second-order expansions.

To push the approximations more to their limit, we now increase the emitter-cavity coupling to $g = 0.086$ eV and again show the emitter population dynamics under short-pulse driving, in Fig. 10, and for a semi-infinite pulse, in Fig. 11. The amplitudes of the classical electric fields and their parameters are the same as in the previous figures. For these parameters, we are approaching the ultrastrong-coupling regime²⁴ as the Rabi splitting $\Omega_R \approx 2g = 0.172$ eV becomes non-negligible compared to the emitter frequency $\Omega_0 = 2.72$ eV. This implies that the counter-rotating terms in the light-matter interaction become important and even the ground state becomes dressed. Although we still choose the uncoupled ground state of the system (EM vacuum and emitter in the ground state) as the initial state, this state is not the ground state of the coupled system, and starting the dynamics immediately leads to fast “quenching” or “ringdown” oscillations at short times. These are seen for weak driving fields in subplots (a) and (b)

of Figs. 10 and 11. Additionally, the very strong coupling implies that the polaritonic states of the coupled cavity-emitter system at $\omega_{\pm} \approx \Omega_0 \pm g$ are now quite strongly detuned from the driving pulse that is tuned to resonance with the bare-emitter (and cavity) resonance frequency. The excitation amplitudes and driven Rabi oscillation frequencies in this case are therefore significantly smaller than for the previously treated systems with smaller light-matter coupling strengths.

We now again investigate the validity of the various approximations. The mean-field approximation cannot represent the ultrastrong-coupling induced changes, which only show up in correlations but do not lead to coherent fields. Therefore, neither the ground state nor the steady state of the system can be described correctly. This is especially noticeable under weak driving [subplots (a) and (b)], where the shape of the driven oscillations is predicted reasonably well, but the final populations are underestimated for both types of driving. The higher-order expansions improve on this result, but not even the third-order approximation manages to fully reproduce the dynamics. This failure is most likely due to the fact that the low-order correlation expansions now have to reproduce both the ultrastrong-coupling induced correlations as well as the driving-pulse induced correlations so that overall, higher-order

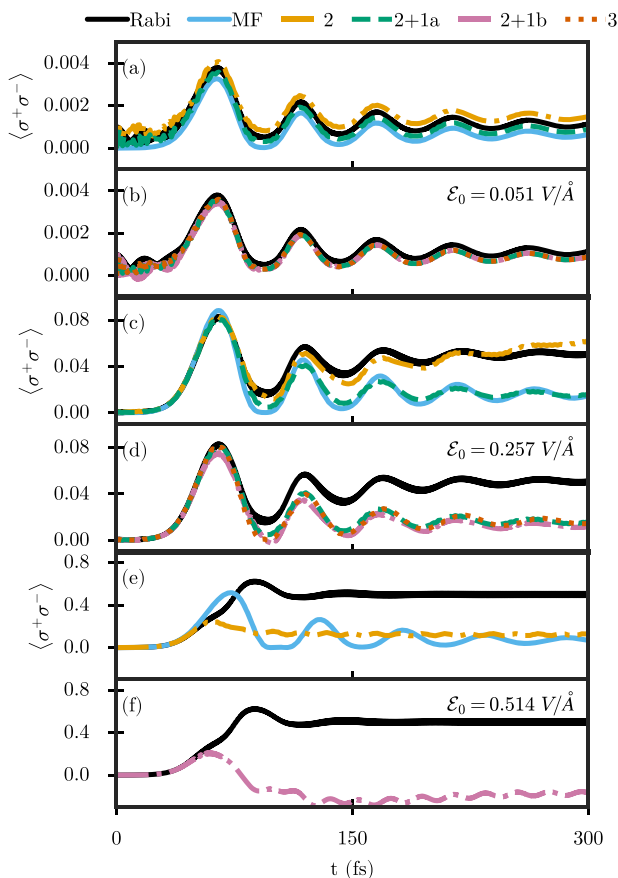


FIG. 11. Same as Fig. 10, but for a semi-infinite driving pulse with constant amplitude after a smooth turn-on.

correlations become more important than in cases with weaker emitter-cavity coupling. Still, under weak driving, all approximations manage to represent the overall dynamics reasonably well up to a global shift. Interestingly, in this case, the 2+1a, 2+1b, and third-order approximations all perform almost identically.

When the driving field amplitude is increased [subplots (c) and (d) in Figs. 10 and 11], the correction to the population due to the counter-rotating terms becomes less noticeable since the laser-induced populations are larger. However, the predictions of the cumulant expansion methods start to diverge more and more from the exact results obtained within the dissipative Rabi model. Here, the (ultra)strong light-matter coupling in combination with the strong driving induces large correlations between light and matter that fail to be described within low-order cumulant expansions. In particular, in the case of the semi-infinite pulse, the results obtained within the cumulant expansion fail to reproduce the steady-state results even qualitatively and lead to significant shifts. It should be noted that these effects are expected to be less relevant when many emitters are included in the cavity.⁷³

For the most intense driving field [subplots (e) and (f) in Figs. 10 and 11], all considered approximations start to break down for the strong emitter-cavity coupling considered here. For the

short-pulse case (Fig. 11), none of the approximations reproduces the Rabi model even qualitatively, with the 2+1b and third-order results again reaching unphysical values of the emitter population, $\langle \sigma^+ \sigma^- \rangle < 0$.

For the case of the semi-infinite pulse (Fig. 11), a similar picture presents itself. For these strong driving pulses, none of the approximations captures the emitter dynamics well. In particular, the simulations using the 2+1a and third-order approximations break down even more dramatically shortly after the start of the pulse, with the emitter population diverging toward infinity. These results are therefore not shown here. We note that, as far as we could determine, these divergences are not due to numerical issues that could be solved by using better integration algorithms but correspond to the actual behavior of the system description at the chosen level and, thus, indicate a complete breakdown of the approximations.

IV. SUMMARY AND OUTLOOK

To summarize, we have explored the cumulant expansion method to calculate the Heisenberg equations of motion for one emitter coupled to an arbitrary number of EM modes with an arbitrary spectral density as obtained through the formalism of macroscopic QED in nanophotonic and plasmonic systems. In order to benchmark the method, we have compared its results to two well-known cases where quasi-exact solutions are available: an emitter in free-space, where perturbative approaches to light-matter coupling are valid, and a Lorentzian spectral density that can be mapped analytically to a Lindblad master equation describing the dissipative Rabi model, i.e., coupling of the emitter to a single cavity mode with losses. In the case of the cavity, we have explored the change in behavior as the coupling strength is increased from the weak up to the ultrastrong-coupling regime. We have investigated both the spontaneous emission dynamics where the emitter is initially excited and the behavior when a classical pulse pumps the system and compared exact solutions with the predictions at different orders of approximation. We have found that, in order to describe spontaneous emission, going beyond the mean-field is essential. While in free space, the second-order approximation is enough to describe, in the cavity, the fact that the photon can be reabsorbed after emission leads to corrections that are only well-described at higher orders of approximation. Here, we have identified a single third-order term that describes the only important contribution at that order, $\langle a_n^\dagger a_m \sigma^z \rangle_C$. In order to describe spontaneous emission correctly (using the approximation we call 2+1b), it is then necessary to explicitly disregard a fourth-order expectation value, instead of performing the cumulant expansion on it. More systematic approximations, such as 2+1a, in which no specific assumptions are made for any the expectation values of the system, cannot describe the spontaneous emission unless higher orders are included in the expansion as some non-negligible correlations arise in the set of equations. For this situation, the correlation expansion does not actually provide a better approximation than working directly with expectation values and discarding higher orders.

As expected, the mean-field approximation is able to describe the emitter dynamics when a classical field pumps the system if

coherent interactions are predominant. In free space, the description is accurate although the slow (nanosecond-scale) spontaneous emission and associated decay after the pulse again cannot be represented. The second-order approximation again can reproduce this decay.

In the strong-coupling regime, i.e., when the emitter is coupled to a cavity mode with coupling strengths similar to or larger than the cavity losses, the second-order approximation fails to describe the dynamics in several cases. The combined action of the coherent driving laser pulse and the strong light–matter coupling with the cavity mode lead to an increase in light–matter correlations at intermediate times which is proportional to both the driving field strength and the light–matter coupling strength. In order to describe these correlations well, the order of the expansion has to be increased, with the third-order expansion being sufficient to describe most investigated cases. At later times, either after the pulse in short-pulse driving or when a steady state is approached under continuous driving, the required order of the approximation needed to describe the system well again decreases. However, for large enough emitter-cavity coupling strengths and driving intensities, the cumulant expansions at the orders used here fail to describe the dynamics and become unstable. In general, the order of approximation or even the validity of the cumulant expansion method to describe the emitter dynamics depends strongly on the physical system and the initial conditions and driving.

Going forward, it would be interesting to study the convergence properties of the cumulant expansion when the number of emitters is increased. In that case, the system is expected to behave more “classically” so that low-order cumulant expansions could provide a better approximation than in the cases studied here, in particular, under driving by external coherent laser pulses. Furthermore, the capability of the method to treat an arbitrary spectral density could be exploited to study emitter dynamics in systems that are not well-described by a single or few cavity modes, such as found in complex nanoplasmonic or hybrid plasmonic-dielectric structures.^{10–13,42}

ACKNOWLEDGMENTS

This work was funded by the European Research Council through Grant No. ERC-2016-StG-714870 and the Spanish Ministry for Science, Innovation, and Universities—Agencia Estatal de Investigación through Grant Nos. RTI2018-099737-B-I00, PCI2018-093145 (through the QuantERA program of the European Commission), and MDM-2014-0377 (through the María de Maeztu program for Units of Excellence in R&D).

APPENDIX A: CUMULANT EXPANSIONS UP TO FOURTH ORDER

For reference, we here give the cumulant expansion for expectation values of products of up to four operators expressed in terms of single-operator expectation values and cumulants,⁵³

$$\langle ab \rangle = \langle ab \rangle_C + \langle a \rangle \langle b \rangle, \quad (\text{A1a})$$

$$\langle abc \rangle = \langle abc \rangle_C + \langle a \rangle \langle b \rangle \langle c \rangle + \langle a \rangle \langle bc \rangle_C + \langle b \rangle \langle ac \rangle_C + \langle c \rangle \langle ab \rangle_C, \quad (\text{A1b})$$

$$\begin{aligned} \langle abcd \rangle &= \langle abcd \rangle_C + \langle a \rangle \langle b \rangle \langle c \rangle \langle d \rangle + \langle a \rangle \langle b \rangle \langle cd \rangle_C + \langle ab \rangle_C \langle c \rangle \langle d \rangle \\ &+ \langle ab \rangle_C \langle cd \rangle_C + \langle a \rangle \langle c \rangle \langle bd \rangle_C + \langle ac \rangle_C \langle b \rangle \langle d \rangle + \langle ac \rangle_C \langle bd \rangle_C \\ &+ \langle a \rangle \langle d \rangle \langle bc \rangle_C + \langle ad \rangle_C \langle b \rangle \langle c \rangle + \langle ad \rangle_C \langle bc \rangle_C + \langle a \rangle \langle bcd \rangle_C \\ &+ \langle b \rangle \langle acd \rangle_C + \langle c \rangle \langle abd \rangle_C + \langle d \rangle \langle abc \rangle_C. \end{aligned} \quad (\text{A1c})$$

APPENDIX B: THIRD-ORDER EQUATIONS

For reference, we here reproduce the equations needed to describe the third-order expectation values,

$$\begin{aligned} \partial_t \langle a_n^\dagger a_m \sigma^x \rangle &= i(\omega_n - \omega_m) \langle a_n^\dagger a_m \sigma^x \rangle - \Omega_0 \langle a_n^\dagger a_m \sigma^y \rangle \\ &+ ig_n \langle a_m \rangle - ig_m \langle a_n^\dagger \rangle, \end{aligned} \quad (\text{B1a})$$

$$\begin{aligned} \partial_t \langle a_n^\dagger a_m \sigma^y \rangle &= i(\omega_n - \omega_m) \langle a_n^\dagger a_m \sigma^y \rangle + \Omega_0 \langle a_n^\dagger a_m \sigma^x \rangle \\ &- g_n \langle a_m \sigma^z \rangle - g_m \langle a_n^\dagger \sigma^z \rangle \\ &- 2 \sum_l g_l \left(\langle a_n^\dagger a_l^\dagger a_m \sigma^z \rangle + \langle a_n^\dagger a_l a_m \sigma^z \rangle \right) \\ &+ 2 \mu \mathcal{E}(t) \langle a_n^\dagger a_m \sigma^z \rangle, \end{aligned} \quad (\text{B1b})$$

$$\begin{aligned} \partial_t \langle a_n^\dagger a_m \sigma^z \rangle &= i(\omega_n - \omega_m) \langle a_n^\dagger a_m \sigma^z \rangle + g_n \langle a_m \sigma^y \rangle + g_m \langle a_n^\dagger \sigma^y \rangle \\ &+ 2 \sum_l g_l \left(\langle a_n^\dagger a_l^\dagger a_m \sigma^y \rangle + \langle a_n^\dagger a_l a_m \sigma^y \rangle \right) \\ &- 2 \mu \mathcal{E}(t) \langle a_n^\dagger a_m \sigma^y \rangle, \end{aligned} \quad (\text{B1c})$$

$$\begin{aligned} \partial_t \langle a_n^\dagger a_m^\dagger \sigma^x \rangle &= i(\omega_n + \omega_m) \langle a_n^\dagger a_m^\dagger \sigma^x \rangle - \Omega_0 \langle a_n^\dagger a_m^\dagger \sigma^y \rangle \\ &+ ig_n \langle a_m^\dagger \rangle + ig_m \langle a_n^\dagger \rangle, \end{aligned} \quad (\text{B1d})$$

$$\begin{aligned} \partial_t \langle a_n^\dagger a_m^\dagger \sigma^y \rangle &= i(\omega_n + \omega_m) \langle a_n^\dagger a_m^\dagger \sigma^y \rangle + \Omega_0 \langle a_n^\dagger a_m^\dagger \sigma^x \rangle \\ &- g_n \langle a_m^\dagger \sigma^z \rangle - g_m \langle a_n^\dagger \sigma^z \rangle \\ &- 2 \sum_l g_l \left(\langle a_n^\dagger a_l^\dagger a_m^\dagger \sigma^z \rangle + \langle a_n^\dagger a_m^\dagger a_l \sigma^z \rangle \right) \\ &+ 2 \mu \mathcal{E}(t) \langle a_n^\dagger a_m^\dagger \sigma^z \rangle, \end{aligned} \quad (\text{B1e})$$

$$\begin{aligned} \partial_t \langle a_n^\dagger a_m^\dagger \sigma^z \rangle &= i(\omega_n + \omega_m) \langle a_n^\dagger a_m^\dagger \sigma^z \rangle + g_n \langle a_m^\dagger \sigma^y \rangle + g_m \langle a_n^\dagger \sigma^y \rangle \\ &+ 2 \sum_l g_l \left(\langle a_n^\dagger a_l^\dagger a_m^\dagger \sigma^y \rangle + \langle a_n^\dagger a_m^\dagger a_l \sigma^y \rangle \right) \\ &- 2 \mu \mathcal{E}(t) \langle a_n^\dagger a_m^\dagger \sigma^y \rangle, \end{aligned} \quad (\text{B1f})$$

$$\begin{aligned} \partial_t \langle a_n^\dagger a_m^\dagger a_l \rangle &= i(\omega_n + \omega_m - \omega_l) \langle a_n^\dagger a_m^\dagger a_l \rangle + ig_n \langle a_m^\dagger a_l \sigma^x \rangle \\ &+ ig_m \langle a_n^\dagger a_l \sigma^x \rangle - ig_l \langle a_n^\dagger a_m^\dagger \sigma^x \rangle, \end{aligned} \quad (\text{B1g})$$

$$\begin{aligned} \partial_t \langle a_n^\dagger a_m^\dagger a_l^\dagger \rangle &= i(\omega_n + \omega_m + \omega_l) \langle a_n^\dagger a_m^\dagger a_l^\dagger \rangle + ig_n \langle a_m^\dagger a_l^\dagger \sigma^x \rangle \\ &+ ig_m \langle a_n^\dagger a_l^\dagger \sigma^x \rangle + ig_l \langle a_n^\dagger a_m^\dagger \sigma^x \rangle. \end{aligned} \quad (\text{B1h})$$

In the approximation 2+1a, just Eq. (B1c) is added to the sets of Eqs. (10) and (11). Moreover, the fourth-order terms are expanded up to second order, so both the fourth and the third order correlations are neglected. The equation of motion of the third-order correlation is

$$\begin{aligned}
\partial_t \langle a_n^\dagger a_m \sigma^z \rangle_C &= g_n \left(\langle a_m \sigma^y \rangle_C - i \langle \sigma^x \rangle_C \langle a_m \sigma^z \rangle_C - i \langle \sigma^z \rangle_C \langle a_m \sigma^x \rangle_C \right) \\
&+ g_m \left(\langle a_n \sigma^y \rangle_C + i \langle \sigma^x \rangle_C \langle a_n^\dagger \sigma^z \rangle_C + i \langle \sigma^z \rangle_C \langle a_n^\dagger \sigma^x \rangle_C \right) \\
&+ i(\omega_n - \omega_m) \langle a_n^\dagger a_m \sigma^z \rangle_C + 2 \sum_l g_l \\
&\times \left(\langle a_l^\dagger a_n^\dagger \rangle_C \langle a_m \sigma^y \rangle_C + \langle a_l^\dagger a_m \rangle_C \langle a_n^\dagger \sigma^y \rangle_C \right. \\
&\left. + \langle a_n^\dagger a_l \rangle_C \langle a_m \sigma^y \rangle_C + \langle a_l a_m \rangle_C \langle a_n^\dagger \sigma^y \rangle_C \right). \quad (\text{B2})
\end{aligned}$$

In Eq. (B2), the terms $\langle a_n^\dagger a_m a_l \sigma^y \rangle_C$, $\langle a_m a_l \sigma^y \rangle_C$, $\langle a_n^\dagger a_l \sigma^y \rangle_C$, and $\langle a_n^\dagger a_m \sigma^y \rangle_C$ are neglected. The correlations inside the last bracket in (B2) make this term non-negligible although the expectation values in (B1c) are analytically zero.

In the approximation 2+1b, Eq. (B1c) is again the only one added, but instead of doing the cumulant expansion of the higher-order terms that appear in this equation, the condition $\langle a_n^\dagger a_l^\dagger a_m \sigma^y \rangle = \langle a_n^\dagger a_l a_m \sigma^y \rangle = 0$ is imposed directly.

REFERENCES

- E. M. Purcell, "Spontaneous emission probabilities at radio frequencies," *Phys. Rev.* **69**, 681 (1946).
- Y. Kaluzny, P. Goy, M. Gross, J. Raimond, and S. Haroche, "Observation of self-induced Rabi oscillations in two-level atoms excited inside a resonant cavity: The ringing regime of superradiance," *Phys. Rev. Lett.* **51**, 1175 (1983).
- R. J. Thompson, G. Rempe, and H. J. Kimble, "Observation of normal-mode splitting for an atom in an optical cavity," *Phys. Rev. Lett.* **68**, 1132 (1992).
- C. Weisbuch, M. Nishioka, A. Ishikawa, and Y. Arakawa, "Observation of the coupled exciton-photon mode splitting in a semiconductor quantum microcavity," *Phys. Rev. Lett.* **69**, 3314 (1992).
- D. G. Lidzey, D. D. C. Bradley, M. S. Skolnick, T. Virgili, S. Walker, and D. M. Whittaker, "Strong exciton-photon coupling in an organic semiconductor microcavity," *Nature* **395**, 53 (1998).
- J. Bellessa, C. Bonnand, J. C. Plenet, and J. Mugnier, "Strong coupling between surface plasmons and excitons in an organic semiconductor," *Phys. Rev. Lett.* **93**, 036404 (2004).
- J. Dintinger, S. Klein, F. Bustos, W. L. Barnes, and T. W. Ebbesen, "Strong coupling between surface plasmon-polaritons and organic molecules in subwavelength hole arrays," *Phys. Rev. B* **71**, 035424 (2005).
- S. R. K. Rodriguez, J. Feist, M. A. Verschuuren, F. J. García Vidal, and J. Gómez Rivas, "Thermalization and cooling of plasmon-exciton polaritons: Towards quantum condensation," *Phys. Rev. Lett.* **111**, 166802 (2013).
- G. Zengin, M. Wersäll, S. Nilsson, T. J. Antosiewicz, M. Käll, and T. Shegai, "Realizing strong light-matter interactions between single-nanoparticle plasmons and molecular excitons at ambient conditions," *Phys. Rev. Lett.* **114**, 157401 (2015).
- R. Chikkaraddy, B. de Nijs, F. Benz, S. J. Barrow, O. A. Scherman, E. Rosta, A. Demetriadou, P. Fox, O. Hess, and J. J. Baumberg, "Single-molecule strong coupling at room temperature in plasmonic nanocavities," *Nature* **535**, 127 (2016).
- R.-Q. Li, D. Hernández-Pérez, F. J. García-Vidal, and A. I. Fernández-Domínguez, "Transformation optics approach to plasmon-exciton strong coupling in nanocavities," *Phys. Rev. Lett.* **117**, 107401 (2016).
- B. Gurlek, V. Sandoghdar, and D. Martín-Cano, "Manipulation of quenching in nanoantenna-emitter systems enabled by external detuned cavities: A path to enhance strong-coupling," *ACS Photonics* **5**, 456 (2018).
- S. Franke, S. Hughes, M. Kamandar Dezfouli, P. T. Kristensen, K. Busch, A. Knorr, and M. Richter, "Quantization of quasinormal modes for open cavities and plasmonic cavity quantum electrodynamics," *Phys. Rev. Lett.* **122**, 213901 (2019).
- A. Bisht, J. Cuadra, M. Wersäll, A. Canales, T. J. Antosiewicz, and T. Shegai, "Collective strong light-matter coupling in hierarchical microcavity-plasmon-exciton systems," *Nano Lett.* **19**, 189 (2019).
- C. Cohen-Tannoudji, J. Roc, and G. Grynberg, *Photons and Atoms: Introduction to Quantum Electrodynamics* (Wiley-Interscience, New York, 1987).
- I. I. Rabi, "Space quantization in a gyrating magnetic field," *Phys. Rev.* **51**, 652 (1937).
- R. Dicke, "Coherence in spontaneous radiation processes," *Phys. Rev.* **93**, 99 (1954).
- E. T. Jaynes and F. W. Cummings, "Comparison of quantum and semiclassical radiation theories with application to the beam maser," *Proc. IEEE* **51**, 89 (1963).
- M. Tavis and F. W. Cummings, "Exact solution for an N-Molecule-Radiation-Field Hamiltonian," *Phys. Rev.* **170**, 379 (1968).
- H. J. Carmichael, *Statistical Methods in Quantum Optics I* (Springer Berlin Heidelberg, Berlin, Heidelberg, 1999).
- C. W. Gardiner and P. Zoller, *Quantum Noise: A Handbook of Markovian and Non-Markovian Quantum Stochastic Methods with Applications to Quantum Optics* (Springer Berlin Heidelberg, 2004).
- G. Grynberg, A. Aspect, C. Fabre, and C. Cohen-Tannoudji, *Introduction to Quantum Optics: From the Semi-Classical Approach to Quantized Light* (Cambridge University Press, Cambridge, 2010).
- B. M. Garraway, "The Dicke model in quantum optics: Dicke model revisited," *Philos. Trans. R. Soc. A* **369**, 1137 (2011).
- A. Frisk Kockum, A. Miranowicz, S. D. Liberato, S. Savasta, and F. Nori, "Ultrastrong coupling between light and matter," *Nat. Rev. Phys.* **1**, 19 (2019).
- A. Pusch, S. Wuestner, J. M. Hamm, K. L. Tsakmakidis, and O. Hess, "Coherent amplification and noise in gain-enhanced nanoplasmonic metamaterials: A Maxwell-Bloch Langevin approach," *ACS Nano* **6**, 2420 (2012).
- M. Sukharev and A. Nitzan, "Optics of exciton-plasmon nanomaterials," *J. Phys.: Condens. Matter* **29**, 443003 (2017).
- H.-T. Chen, T. E. Li, M. Sukharev, A. Nitzan, and J. E. Subotnik, "Ehrenfest+R dynamics. I. A mixed quantum-classical electrodynamic simulation of spontaneous emission," *J. Chem. Phys.* **150**, 044102 (2019).
- H.-T. Chen, T. E. Li, M. Sukharev, A. Nitzan, and J. E. Subotnik, "Ehrenfest+R dynamics. II. A semiclassical QED framework for Raman scattering," *J. Chem. Phys.* **150**, 044103 (2019).
- N. M. Hoffmann, C. Schäfer, A. Rubio, A. Kelly, and H. Appel, "Capturing vacuum fluctuations and photon correlations in cavity quantum electrodynamics with multitrajjectory Ehrenfest dynamics," *Phys. Rev. A* **99**, 063819 (2019).
- A. Trügler and U. Hohenester, "Strong coupling between a metallic nanoparticle and a single molecule," *Phys. Rev. B* **77**, 115403 (2008).
- E. Waks and D. Sridharan, "Cavity QED treatment of interactions between a metal nanoparticle and a dipole emitter," *Phys. Rev. A* **82**, 043845 (2010).
- B. Huttner and S. M. Barnett, "Quantization of the electromagnetic field in dielectrics," *Phys. Rev. A* **46**, 4306 (1992).
- S. Scheel, L. Knöll, and D.-G. Welsch, "QED commutation relations for inhomogeneous Kramers-Kronig dielectrics," *Phys. Rev. A* **58**, 700 (1998).
- S. Scheel and S. Y. Buhmann, "Macroscopic quantum electrodynamics—Concepts and applications," *Acta Phys. Slovaca* **58**, 675 (2008).
- S. Y. Buhmann, *Dispersion Forces I*, Springer Tracts in Modern Physics Vol. 247 (Springer Berlin Heidelberg, Berlin, Heidelberg, 2012).
- H. T. Dung, L. Knöll, and D.-G. Welsch, "Three-dimensional quantization of the electromagnetic field in dispersive and absorbing inhomogeneous dielectrics," *Phys. Rev. A* **57**, 3931 (1998).
- M. Wubs, L. G. Suttorp, and A. Lagendijk, "Multiple-scattering approach to interatomic interactions and superradiance in inhomogeneous dielectrics," *Phys. Rev. A* **70**, 053823 (2004).
- S. Y. Buhmann, *Dispersion Forces II*, Springer Tracts in Modern Physics Vol. 248 (Springer Berlin Heidelberg, Berlin, Heidelberg, 2012).
- A. Delga, J. Feist, J. Bravo-Abad, and F. J. García-Vidal, "Quantum emitters near a metal nanoparticle: Strong coupling and quenching," *Phys. Rev. Lett.* **112**, 253601 (2014).
- S. Y. Buhmann and D.-G. Welsch, "Casimir-Polder forces on excited atoms in the strong atom-field coupling regime," *Phys. Rev. A* **77**, 012110 (2008).
- T. Hümmer, F. J. García-Vidal, L. Martín-Moreno, and D. Zueco, "Weak and strong coupling regimes in plasmonic QED," *Phys. Rev. B* **87**, 115419 (2013).

- ⁴²B. Rousseaux, D. Dzsotjan, G. Colas des Francs, H. R. Jauslin, C. Couteau, and S. Guérin, “Adiabatic passage mediated by plasmons: A route towards a decoherence-free quantum plasmonic platform,” *Phys. Rev. B* **93**, 045422 (2016).
- ⁴³L. Novotny and B. Hecht, *Principles of Nano-Optics*, 2nd ed. (Cambridge University Press, Cambridge, 2012).
- ⁴⁴A. González-Tudela, P. A. Huidobro, L. Martín-Moreno, C. Tejedor, and F. J. García-Vidal, “Reversible dynamics of single quantum emitters near metal-dielectric interfaces,” *Phys. Rev. B* **89**, 041402(R) (2014).
- ⁴⁵A. Cuartero-González and A. I. Fernández-Domínguez, “Light-forbidden transitions in plasmon-emitter interactions beyond the weak coupling regime,” *ACS Photonics* **5**, 3415 (2018).
- ⁴⁶I. de Vega and D. Alonso, “Dynamics of non-Markovian open quantum systems,” *Rev. Mod. Phys.* **89**, 015001 (2017).
- ⁴⁷U. Schollwöck, “The density-matrix renormalization group in the age of matrix product states,” *Ann. Phys.* **326**, 96 (2011).
- ⁴⁸F. A. Y. N. Schröder, D. H. P. Turban, A. J. Musser, N. D. M. Hine, and A. W. Chin, “Tensor network simulation of multi-environmental open quantum dynamics via machine learning and entanglement renormalisation,” *Nat. Commun.* **10**, 1062 (2019).
- ⁴⁹Y. Tanimura, “Nonperturbative expansion method for a quantum system coupled to a harmonic-oscillator bath,” *Phys. Rev. A* **41**, 6676 (1990).
- ⁵⁰A. W. Chin, Á. Rivas, S. F. Huelga, and M. B. Plenio, “Exact mapping between system-reservoir quantum models and semi-infinite discrete chains using orthogonal polynomials,” *J. Math. Phys.* **51**, 092109 (2010).
- ⁵¹J. del Pino, F. A. Y. N. Schröder, A. W. Chin, J. Feist, and F. J. García-Vidal, “Tensor network simulation of polaron-polaritons in organic microcavities,” *Phys. Rev. B* **98**, 165416 (2018).
- ⁵²J. del Pino, F. A. Y. N. Schröder, A. W. Chin, J. Feist, and F. J. García-Vidal, “Tensor network simulation of non-Markovian dynamics in organic polaritons,” *Phys. Rev. Lett.* **121**, 227401 (2018).
- ⁵³R. Kubo, “Generalized cumulant expansion method,” *J. Phys. Soc. Jpn.* **17**, 1100 (1962).
- ⁵⁴M. Kira and S. W. Koch, “Cluster-expansion representation in quantum optics,” *Phys. Rev. A* **78**, 022102 (2008).
- ⁵⁵M. Kira and S. W. Koch, *Semiconductor Quantum Optics* (Cambridge University Press, Cambridge, 2011).
- ⁵⁶K. Henshel, J. Majer, J. Schmiedmayer, and H. Ritsch, “Cavity QED with an ultracold ensemble on a chip: Prospects for strong magnetic coupling at finite temperatures,” *Phys. Rev. A* **82**, 033810 (2010).
- ⁵⁷P. Kirton and J. Keeling, “Superradiant and lasing states in driven-dissipative Dicke models,” *New J. Phys.* **20**, 015009 (2018).
- ⁵⁸N. M. Hoffmann, C. Schäfer, N. Säkkinen, A. Rubio, H. Appel, and A. Kelly, “Benchmarking semiclassical and perturbative methods for real-time simulations of cavity-bound emission and interference,” *J. Chem. Phys.* **151**(24), 244113 (2019).
- ⁵⁹M. Zens, D. O. Krimer, and S. Rotter, “Critical phenomena and nonlinear dynamics in a spin ensemble strongly coupled to a cavity. II. Semiclassical-to-Quantum boundary,” *Phys. Rev. A* **100**, 013856 (2019).
- ⁶⁰A. W. Chin, S. F. Huelga, and M. B. Plenio, “Chain representations of open quantum systems and their numerical simulation with time-adaptive density matrix renormalisation group methods,” in *Semiconductors and Semimetals* (Elsevier, Inc., 2011), Vol. 85, p. 115.
- ⁶¹In principle, this is not the ground state of the full system, as we include counter-rotating terms in the light-matter coupling, and thus ultrastrong-coupling effects such as ground-state modifications.²⁴ For the cases we treat below, the error due to this approximation is negligible.
- ⁶²J. Feist, <https://github.com/jfeist/QuantumAlgebra.jl>, 2019.
- ⁶³J. Bezanson, A. Edelman, S. Karpinski, and V. B. Shah, “Julia: A fresh approach to numerical computing,” *SIAM Rev.* **59**, 65 (2017).
- ⁶⁴C. Rackauckas and Q. Nie, “DifferentialEquations.jl—A performant and feature-rich ecosystem for solving differential equations in Julia,” *J. Open Res. Software* **5**, 15 (2017).
- ⁶⁵D. A. Steck, *Quantum and Atom Optics* (unpublished), available at <http://steck.us/teaching>.
- ⁶⁶V. Weisskopf and E. Wigner, “Über die natürliche linienbreite in der strahlung des harmonischen oszillators,” *Z. Phys. Hadrons Nucl.* **65**, 18 (1930).
- ⁶⁷J. Andreasen and H. Cao, “Finite-difference time-domain formulation of stochastic noise in macroscopic atomic systems,” *J. Lightwave Technol.* **27**, 4530 (2009).
- ⁶⁸P. Törmä and W. L. Barnes, “Strong coupling between surface plasmon polaritons and emitters: A review,” *Rep. Prog. Phys.* **78**, 013901 (2015).
- ⁶⁹L. Allen and J. H. Eberly, *Optical Resonance and Two-Level Atoms* (Dover, New York, 1987).
- ⁷⁰J. Cuerda, F. J. García-Vidal, and J. Bravo-Abad, “Spatio-temporal modeling of lasing action in core-shell metallic nanoparticles,” *ACS Photonics* **3**, 1952 (2016).
- ⁷¹J. Cuerda, F. Rütting, F. J. García-Vidal, and J. Bravo-Abad, “Theory of lasing action in plasmonic crystals,” *Phys. Rev. B* **91**, 041118(R) (2015).
- ⁷²D. M. Coles, N. Somaschi, P. Michetti, C. Clark, P. G. Lagoudakis, P. G. Savvidis, and D. G. Lidzey, “Polariton-mediated energy transfer between organic dyes in a strongly coupled optical microcavity,” *Nat. Mater.* **13**, 712 (2014).
- ⁷³P. Kirton and J. Keeling, “Suppressing and restoring the Dicke superradiance transition by dephasing and decay,” *Phys. Rev. Lett.* **118**, 123602 (2017).